Elsevier Editorial System(tm) for Science of the Total Environment
Manuscript Draft

Manuscript Number: STOTEN-D-20-09841R2

Title: Natural springs protection and probabilistic risk assessment under uncertain conditions.

Article Type: Research Paper

Keywords: Groundwater management, Natural springs, Probabilistic risk assessment, Model and parameter uncertainty, Decision-making

Corresponding Author: Dr. Emanuela Bianchi Janetti,

Corresponding Author's Institution: Politecnico di Milano

First Author: Emanuela Bianchi Janetti

Order of Authors: Emanuela Bianchi Janetti; Monica Riva; Alberto Guadagnini

Abstract: The study introduces a comprehensive framework for natural springs' protection and probabilistic risk assessment in the presence of uncertainty associated with the characterization of the groundwater system. The methodology is applied to a regional-scale hydrogeological setting, located in Northern Italy and characterized by the presence of high-quality natural springs forming a unique system whose preservation is of critical importance for the region. Diverse risk pathways are presented to constitute a fault tree model enabling identification of all basic events, each associated with uncertainty and contributing to an undesired system failure. The latter is quantified in terms of hydraulic head falling below a given threshold value for at least one amongst all active springs. The workflow explicitly includes the impact of model parameter uncertainty on the evaluation of the overall probability of system failure due to alternative groundwater extraction strategies. To cope with conceptual model uncertainty, two models based on different reconstructions of the aquifer geological structure are considered. In each conceptual model, hydraulic conductivities related to the geomaterials composing the aquifer are affected by uncertainty. It is found that (a) the type of conceptual model employed to characterize the aquifer structure strongly affects the probability of system failure and (b) uncertainties associated with the ensuing conductivity fields, even as constrained through model calibration, lead to different impacts on the variability of hydraulic head levels at the springs depending on the conceptual model adopted. The results of the study demonstrate that the proposed approach enables one to (i) quantify the risk associated with springs depletion due to alternative strategies of aquifer exploitation; (ii) quantify the way diverse sources of uncertainty (i.e., model and parameter uncertainty) affect the probability of system failure; (iii) determine the optimal exploitation strategy ensuring system functioning; and (iv) identify the most vulnerable springs, where depletion first occurs.

Response to Reviewers: The detailed response to each Reviewer comments is provided in the attached file 'Response to Reviewers.docx'

*Graphical Abstract

Graphical abstract

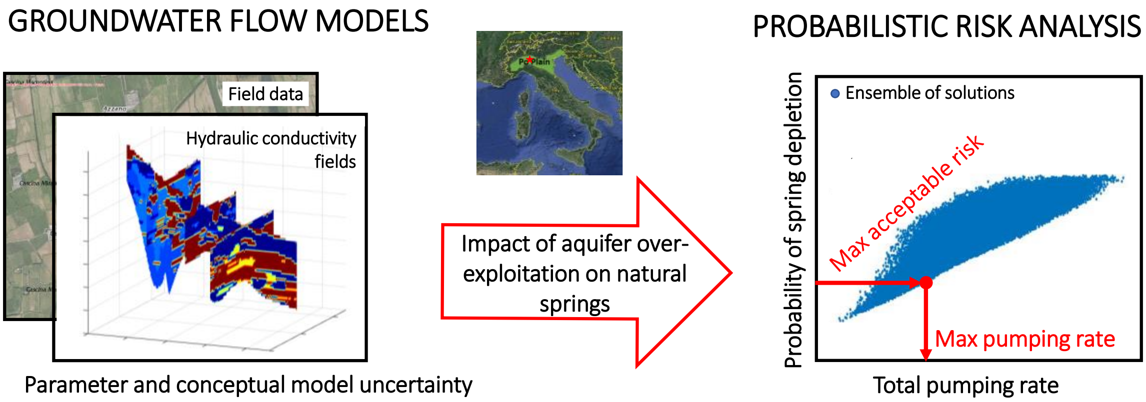

***Highlights (for review : 3 to 5 bullet points (maximum 85 characters including spaces per bullet point)**

Highlights:

- Probability of spring discharge reduction due to aquifer exploitation is quantified
- Multiple sources of uncertainty are considered using a Fault Tree methodology
- The approach balances conflicting goals under parameter and conceptual uncertainty

Natural springs protection and probabilistic risk assessment under uncertain conditions.

Emanuela Bianchi Janetti*[(1)], Monica Riva[(1)], Alberto Guadagnini[(1)]

[(1)] Dipartimento di Ingegneria Civile e Ambientale (DICA), Politecnico di Milano, Piazza Leonardo da Vinci 32, 20133 Milano, Italy

* Corresponding author. Tel. +390223996293 Fax. +390223996298

E-mail address: emanuela.bianchi@polimi.it

Keywords: Groundwater management, Natural springs, Probabilistic risk assessment, Model and parameter uncertainty, Decision-making

Highlights:

- Probability of spring discharge reduction due to aquifer exploitation is quantified
- Multiple sources of uncertainty are considered using a Fault Tree methodology
- The approach balances conflicting goals under parameter and conceptual uncertainty

Abstract

The study introduces a comprehensive framework for natural springs' protection and probabilistic risk assessment in the presence of uncertainty associated with the characterization of the groundwater system. The methodology is applied to a regional-scale hydrogeological setting, located in Northern Italy and characterized by the presence of high-quality natural springs forming a unique system whose preservation is of critical importance for the region. Diverse risk pathways are presented to constitute a fault tree model enabling identification of all basic events, each associated with uncertainty and contributing to an undesired system failure. The latter is quantified in terms of hydraulic head falling below a given threshold value for at least one amongst all active springs. The workflow explicitly includes the impact of model parameter uncertainty on the evaluation of the overall probability of system failure due to alternative groundwater extraction strategies. To cope with conceptual model uncertainty, two models based on different reconstructions of the aquifer geological structure are considered. In each conceptual model, hydraulic conductivities related to the geomaterials composing the aquifer are affected by uncertainty. It is found that (*a*) the type of conceptual model employed to characterize the aquifer structure strongly affects the probability of system failure and (*b*) uncertainties associated with the ensuing conductivity fields, even as constrained through model calibration, lead to different impacts on the variability of hydraulic head levels at the springs depending on the conceptual model adopted. The results of the study demonstrate that the proposed approach enables one to (*i*) quantify the risk associated with springs depletion due to alternative strategies of aquifer exploitation; (*ii*) quantify the way diverse sources of uncertainty (i.e., model and parameter uncertainty) affect the probability of system failure; (*iii*) determine the optimal exploitation strategy ensuring system functioning; and (*iv*) identify the most vulnerable springs, where depletion first occurs.

1. Introduction

Population growth, urbanization and the pursuit of improved living conditions accelerate the need for water, food and energy. Freshwater is a limited resource (only 0.7% of the global water resource is readily available as freshwater) and its availability is a key driver of population dynamics. Groundwater, which is the main source of available freshwater in many countries worldwide (Filimonau and Barth, 2016), is a strategic resource for drinking water supply and is essential for ecosystem quality, energy and food security. Groundwater is at risk from a variety of causes, including over-abstraction, with about 20% of the world's aquifers being estimated to be suffering from over-exploitation (e.g., Amanambu et al., 2020, Jia et al., 2020, Jia et al., 2019, Castellazzi et al., 2016, Gleeson et al., 2012). Groundwater abstraction close to natural springs, which represent key elements of a hydrological system, requires an appraisal and quantification of possible interference between pumping and head levels at the springs, as well as an assessment of the complexity of environmental, social and economic aspects (e.g., Obolewsky at al., 2016, Epting et al., 2018, Liu et al., 2018, Luo et al., 2020). For these reasons, groundwater exploitation and management should foresee relying on an approach that enables considering the coexistence of multiple (sometimes conflicting) objectives.

It is widely recognized that uncertainty affects all efforts to model hydrogeological systems. Aquifer heterogeneity and incomplete knowledge of key attributes enabling site characterization are some of the reasons why decisions about groundwater exploitation and management needs to be made under uncertainty. Decisions are typically informed by several alternatives which are rendered through models plagued by diverse sources of uncertainties. Therefore, risk analysis, which is by its nature interconnected with the concept of uncertainty, must be an integral part of any decision-making process associated with environmental scenarios (Bolster et al., 2009, Tartakovsky, 2013). A Probabilistic Risk Assessment (PRA) allows identifying all basic events and possible risk pathways contributing to an undesired system failure in order to quantify the probability that such an event takes place (Bedford and

Cooke, 2003). This quantitative tool takes advantage of information from multiple entries of various origins and synthesize these in a descriptive and simplified set of indicators, easily transferable to decision makers. Several works show that PRA is a valuable tool for evaluating diverse groundwater-related types of risks, such as, e.g., (*a*) probability of failure of a given groundwater remediation strategy (e.g., Tartakovsky, 2007; Bolster et al., 2009, Fernàndez-Garcia et al., 2012, Siirila-Woodburn et al., 2015), (*b*) events associated with construction of underground structures and their feedbacks with aquifers (Jurado et al., 2011), and (*c*) maintenance of artificial recharge ponds (Pedretti et al., 2011). PRA has also been employed to embed the reconstruction of probabilistic well capture zones (Rodak et al., 2011) and to evaluate human health risk due to toxic chemical cocktails released in groundwater (Henri et al., 2015).

In this broad context, the development of a structured PRA associated with scenarios of spring discharge reduction (possibly leading to spring depletion) linked to groundwater over-abstraction is still lacking. Luo et al. (2020) propose a multi-objective simulation/optimization framework to assess an optimal strategy which balances groundwater extraction and outflow rate at the Baotu spring field, in Northern China. In this study, the authors do not include the effects of any source of uncertainty, the latter being ubiquitous in the representation of subsurface flow and transport processes. Additional studies about springs and their interconnection with groundwater exploitation mainly focus on the analysis of the relationships among spring flow, precipitation, and groundwater abstraction, with the main objective of providing an appraisal, within a deterministic framework, of variations of spring flow due to climate change and human activities (Kang et al., 2011, Zhang et al., 2017, Liu et al 2018).

Our key objective is the development of a methodology to quantify the probability of system failure associated with the reduction of discharge at natural springs due to aquifer over-exploitation in the presence of multiple sources of uncertainty. This is accomplished by relying on a Fault Tree approach.

The applicability and performance of the proposed approach and ensuing operational workflow are shown in an exemplary setting comprising a complex, large scale aquifer system located in Northern Italy. The target aquifer is characterized by the presence of high-quality natural springs which constitute the main supply to agriculture and are a key environmental driver for various activities, forming a unique and highly valuable system whose preservation is of critical importance for the region. As an additional distinctive element, our study provides a solid probabilistic framework for the assessment of the best compromise one can obtain by balancing two conflicting goals, as given by the minimization of the probability of system failure (identified through a reduction of spring discharge below a given threshold) and the maximization of the water volume that can be extracted from the aquifer, under uncertain conditions.

2. Study area and groundwater flow model

The study is focused on a highly heterogeneous regional-scale sedimentary aquifer, located in Northern Italy (see Fig. 1). The main hydrogeological features of the system that are essential to the scope of the present work are illustrated in the following and one can refer to Bianchi Janetti et al. (2019) for additional details, including the exhaustive description of the available data upon which our analyses are grounded.

The considered region is part of the high-medium Alluvial Po Plain in Northern Italy and extends across a planar surface of about 785 km^2. It is located between the two major rivers (Adda and Serio) in the area and hosts activities linked to agricultural (84%) and urban (16%) sectors. The presence of high-quality water springs constitutes a key feature of the system. These natural springs are major environmental drivers and constitute the main water supply for agriculture, which is an important anthropogenic activity in the area.

Main features of the system are depicted in Fig. 1b, which includes the overall pattern of the groundwater surface elevation as well as the location of springs and of pumping wells considered. The aquifer is characterized by an average thickness of about 120 m (stratigraphic data being available up to a depth of about 300 m in some areas) and comprises a free-surface (with a few locally semi-confined conditions) and a deep aquifer. Following Bianchi Janetti et al. (2019), a steady-state groundwater flow pattern, which is taken to represent an average system behavior, is here considered. This choice is consistent with the analysis of the series of piezometric records available in the area from 2004 to 2015. As an example, the yearly-averaged (from 2004 to 2015) hydraulic heads at four observation wells used for model calibration are depicted in Fig. 1c (the exact position of these observation points is included in Fig. 1b). This figure shows that the interannual variability of hydraulic head is negligible within the investigated temporal window. This is also consistent with the purpose of our study, which is to provide a quantitative tool to support decision makers in the context of management of large-scale groundwater resources. As mentioned in Section 1, this is accomplished by developing a methodology conducive to evaluating the probability of system failure accounting for diverse conceptualizations of the hydrogeological domain and the uncertainty of the associated hydraulic parameters governing groundwater flow patterns. Our analysis provides information about the mean behavior of the system on a yearly basis that can be used for a high-level management purpose upon which one can then prioritize requirements for more detailed, local-scale analyses.

In addition, one can also note that for the purpose and level of the risk analysis here considered the steady-state condition can be viewed as a conservative scenario with respect to a transient regime, as it is associated with the largest drawdown produced by the system of pumping wells.

Numerical analyses presented in Section 3 rely on the widely used and tested computational suite MODFLOW-2005 (Harbaugh, 2005). Boundary conditions correspond to (*a*) a total flow rate of 9.65 m^3/s entering the domain from the Northern boundary and (*b*) a Dirichlet boundary conditions imposed along the Adda and Serio rivers which is set to 3 m above the river bottom elevation, consistent with the mean river bank elevation. The aquifer system of extent 23 km (East-West direction) × 48 km

(North-South direction) × 475 m (depth) is discretized through blocks of uniform size of 100 m × 200 m × 5 m, according to available information and computational resources, for a total of 5.2 million voxels. Inactive cells are inserted to reconstruct the topographic surface of the area and the bottom of the system, resulting in about one million active cells. Recharge terms included in the study comprise infiltration from precipitation, irrigation and percolation from channels in the non-urban zones, or aqueduct and sewage system losses in the urban sector. Since exhaustive and up-to-date records detailing the exact location of the pumping wells are not available, for the illustration of our approach, and considering the spatial extent of the system, the total water withdrawal within a given municipality is assigned to a system of wells located at the center of the municipality itself. Springs are simulated as drains, their outflow-rate being proportional to the difference between hydraulic head at the spring cell and elevation of ground level. Additional details are reported in Bianchi Janetti et al. (2019). Consistent with these authors, uncertainty in the conceptual model employed to characterize the subsurface architecture and the spatial variability of hydraulic conductivities in the domain are considered and two conceptual models are implemented according to the steps summarized in the following.

On the basis of available data (see Bianchi Janetti et al., 2019), a set of n_f = 5 main geomaterials (facies) which constitute the geological makeup of the system is identified. Each facies, here denoted as M_i (i = 1, ..., n_f), is listed in Table 1 together with the corresponding volumetric fraction, f_i, assessed from data collected from boreholes within the study area.

The three-dimensional distribution of facies within the system is obtained according to two conceptual models, which are taken to exemplify the way uncertainty about our knowledge of the internal structure of the aquifer system can be embedded in the probabilistic analysis workflow, other types of conceptual models being compatible with our approach. These are termed as *Composite Medium* (*CM*) and *Overlapping Continua* (*OC*) model (see also Bianchi Janetti et al., 2019). According to the *CM* approach (e.g., Winter et al., 2003; Guadagnini et al., 2004 and references therein) a single geomaterial with conductivity $K_j^{CM} = k_i$ (index *i* identifying the facies attributed to voxel *j*) is assigned to each voxel of the numerical model. In essence, this can be seen as corresponding to a zonation of the domain where (in principle) there might be uncertainty in the spatial distributions of the geomaterials and in the value of their hydraulic parameters. The *OC* model is grounded on the concept that the system can be viewed as a collection of media of differing properties coexisting in space. The idea underlying this concept is that each voxel *j* of the numerical grid represents a finite volume within which all geomaterials can coexist, each being associated with a given volumetric fraction, $I_{i,j}$. Hydraulic conductivity at voxel *j* is evaluated as a weighted arithmetic mean of facies conductivities, i.e., $K_j^{OC} = \sum_{i=1}^{n_f} I_{i,j}\, k_i$, (with $\sum_{i=1}^{n_f} I_{i,j} = 1,\ \forall j$).

The *CM* and *OC* conceptual models have also been employed by Bianchi Janetti et al. (2019) who rely on a number of global sensitivity analysis (GSA) techniques to assess the influence of uncertain model parameters on the distribution of hydraulic heads in the complex domain considered. These authors identified the set of hydraulic parameters which are most influential to hydraulic head distributions as log-conductivity values associated with (*i*) clay, gravel, and fractured conglomerate for *CM* and (*ii*) gravel and fractured conglomerate for *OC*. Here, we perform model calibration by taking advantage of these results, the parameters to be estimated corresponding to N_p = 3 and N_p = 2 values of $Y_i = log\ k_i$ (i = 1, ..., N_p) for *OC* and *CM*, respectively. Entries Y_i of vector $\mathbf{Y}$ are estimated through a Maximum Likelihood (ML) approach (Carrera and Neumann, 1986), yielding a ML estimate $\boldsymbol{\mu}$ of $\mathbf{Y}$ based on hydraulic head measurements (see Appendix A for details) as well as a the posterior covariance matrix, $\boldsymbol{\Sigma}$, of the corresponding estimation error.

3. Probabilistic Risk Assessment of the natural springs - groundwater system

Development and application of the PRA requires introducing the following set of components (see, e.g., Tartakovsky, 2013):

(1) *Model predictions*, here identified as the system response in terms of hydraulic head values (h) at a given spring location. Values of h are obtained upon relying on the representation of the groundwater flow system described in Section 2, as implemented according to the two conceptual models considered.

(2) *System Failure* (*SF*) event, here identified with the depletion of at least one spring within the domain. Note that *SF* generally depends on economical/social constraints and its quantification benefits from feedbacks with local stakeholders and decision makers. For the purpose of our exemplary analysis, and considering that the area examined is characterized by a high social impact related to industrial and agricultural activities, our PRA is implemented with the constrain that hydraulic head of all active springs does not fall below a given threshold value, to guarantee a minimum flow rate at each spring.

(3) *Design variables*, here associated with the operational flow rates at a set of selected pumping wells within the domain.

(4) *Sources of uncertainty*, representing our incomplete knowledge about system functioning. Here, two sources of uncertainty are considered, as given by (*i*) the conceptual model employed to represent the system and (*ii*) its ensuing model parameters. Conceptual model uncertainty is included by considering two diverse approaches (i.e., the *CM* and *OC* models described above) to reconstruct the main hydrogeological features of the system. Model parameter uncertainty is tackled by considering the N_p log-conductivity values associated with each of these conceptual models to be characterized by a multivariate Gaussian distribution with mean $\boldsymbol{\mu}$ and covariance $\boldsymbol{\Sigma}$. Evaluation of the latter is grounded on an inverse modeling framework performed within a ML

approach (see Section 2), where the prior error vector and the posterior residual vector ($\mathbf{Y} - \boldsymbol{\mu}$) are assumed to be multivariate Gaussian.

Note that the nature of our study is mainly methodological and is then rendered through an exemplary application scenario. In this context, results from a participatory process with local authorities and stakeholders to refine elements and values for system failure and/or the possibility to broaden the portfolio of scenarios of interest, for example including additional conceptual models and/or adding different types of sources of uncertainty are fully compatible with the presented framework and it is envisioned to tackle these elements in the context of future investigations.

3.1 Fault tree analysis

The probability associated with *SF*, *P*[*SF*], stemming from the combination of the various sources of uncertainty illustrated above can be evaluated through a Fault Tree Analysis (FTA) (e.g., Bedford and Cooke, 2003; Tartakovsky, 2007; Fernàndez-Garcia et al., 2012). A Fault Tree is formed by considering various potential events, whose inter-connections can be represented with Boolean operators. Once a Fault Tree is constructed, the probability of each event must be evaluated, thus enabling assessment of the overall probability that *SF* takes place. As described above, *SF* is here associated with the occurrence of hydraulic head values dropping below an imposed threshold, h_{TR}, at least in one spring (amongst those considered in the analysis), i.e.,

$$h_j\left(\mathbf{Q},\mathbf{Y}\right) - h_{TR,j} < 0 \qquad j = 1,\ldots,N_s \tag{1}$$

Here $\mathbf{Q}$ is a vector containing the flow rate of each pumping well, $h_j\left(\mathbf{Q},\mathbf{Y}\right)$ is hydraulic head evaluated at spring *j* while wells are operating at the pumping flow rate $\mathbf{Q}$ within the log-conductivity field reconstructed (according to the *CM* or *OC* model) upon relying on vector $\mathbf{Y}$ (containing log-conductivity values of each geomaterial), $h_{TR,j}$ is the threshold (minimum hydraulic head) value associated with the j-th spring, and N_s is the number of springs. Values of the entries of $\mathbf{Q}$ vary within the interval $\left[\mathbf{Q}^{\min}, \mathbf{Q}^{\max}\right]$, $\mathbf{Q}^{\min}$ and $\mathbf{Q}^{\max}$ denoting vectors whose entries correspond to the lower ($Q_w^{\min}$) and upper ($Q_w^{\max}$) bounds of Q_w (with w = 1,…, N_w), where N_w is the number of pumping wells in the system.

The outflow-rate of the j-th spring, $Q_{s,j}$, of planar area A_j is then evaluated as

$$Q_{s,j} = \begin{cases} A_j \dfrac{K_{d,j}}{e_j}\left(h_j - h_{0,j}\right) & h_j > h_{0,j} \\ 0 & h_j \le h_{0,j} \end{cases} \tag{2}$$

where $h_{0,j}$ is elevation of the spring bottom, $K_{d,j}$ and e_j being hydraulic conductivity and thickness of the draining bed of the spring, respectively. Knowledge of quantities $K_{d,j}$ and e_j allows evaluating the leakage coefficient $l_{d,j} = K_{d,j}/e_j$, which is here considered as constant (and denoted as l_d) for each spring. The value of l_d has been estimated following calibration of each conceptual model illustrated in Section 2 on the basis of available data about the total discharge from the springs (see Appendix A). The threshold value $h_{TR,j}$ has been evaluated from (2) to ensure a minimum flow rate, $Q_{s,j}^{\min}$, as

$$h_{TR,j} = h_{0,j} + \frac{Q_{s,j}^{\min}}{A_j\, l_d} \tag{3}$$

Along the lines of what noted above, it is observed that the specific value of $Q_{s,j}^{\min}$ to be employed in the probabilistic risk analysis can vary for each spring, eventually including elements associated with economic and social constraints. For simplicity and ease of illustration we consider the same value of $Q_{s,j}^{\min}$ for each spring, hereafter denoted as $Q_s^{\min}$, and also choose to employ the same values for the lower and upper bounds of the flow rate extracted at each of the wells considered in the analysis, hereafter denoted $Q^{\min}$ and $Q^{\max}$.

The construction of the Fault Tree is organized upon partitioning the N_p-dimensional parameter space **Y** (geomaterial log-conductivities) according to the three following regions: (*i*) Region A (Y_A), which comprises the subset of combinations of log-conductivity values for which the constraint (1) is never satisfied; in other words, this region is formed by the collection of the combinations of log-conductivity values for which depletion of at least one spring is observed even under conditions corresponding to the minimum pumping rate ($Q^{\min}$) being set at all pumping wells (i.e., *SF* is always detected); (*ii*) Region C (Y_C) comprises the subset of log-conductivity values for which constraint (1) is satisfied upon setting the maximum pumping rate ($Q^{\max}$) at all pumping wells, i.e., *SF* is never detected; finally (*iii*) Region B (Y_B) includes all combinations of values of geomaterial log-conductivities which do not belong to either Region A or C, i.e., in this case the occurrence of *SF* depends on the values of pumping rate assigned to each well.

The chain of events leading to *SF* is graphically depicted through the Fault Tree included in Fig. 2. The Boolean operators AND and OR applied to two given events *X* and *Z* are expressed according to the following notation: $X \text{ AND } Z \equiv X \cdot Z$ and $X \text{ OR } Z \equiv X + Z$. Therefore, the Boolean expression corresponding to the Fault Tree in Fig. 2 is

$$SF = M_1 + M_2 = Y_A + Y_B \cdot \left(h_{TR,j} > h_j \right) \tag{4}$$

Equation (4) allows identifying the failure modes (M_1 and M_2) of our system (also termed as *minimal cut sets of the system*) and correspond to the smallest collections of events leading to *SF*:

- M_1: {‘Values of geomaterial log-conductivities belong to Region A’}

- M_2: {'Values of geomaterial log-conductivities belong to Region B' AND 'Hydraulic head rendered by the model is lower than the threshold for at least one spring'}.

The probability of *SF*, *P*[*SF*], is then evaluated by the inclusion-exclusion law of probability as

$$P[SF] = P[M_1] + P[M_2] - P[M_1 \cdot M_2] \tag{5}$$

Sampling *N* times the parameter space **Y** yields

$$P[M_1] = P[Y_A] = N_A / N \tag{6}$$

$$P[M_2] = N_B / N \cdot P\left[h_{TR,j} > h_j \right] \tag{7}$$

Here, N_A and N_B indicate the number of sampling points in Region A and Region B, respectively. Since $Y_A \cap Y_A = \varnothing$ (empty set), M_1 and M_2 do not overlap and

$$P[M_1 \cdot M_2] = 0 \tag{8}$$

Substituting (6) - (8) into (5) finally yields

$$P\left[SF\right] = \frac{N_A}{N} + \frac{N_B}{N} \cdot P\left[h_{TR,j} > h_j \right] \tag{9}$$

3.2 Computation of probabilities

To evaluate the probability of system failure (9), the methodology described below and shown in the flow chart depicted in Fig. 3 is then implemented.

(1) A number of *N* Monte Carlo realizations of **Y**, $\mathbf{Y}_n$ (with *n* = 1,…, *N*), characterized by a multivariate Gaussian distribution with mean $\boldsymbol{\mu}$ and covariance $\boldsymbol{\Sigma}$ estimated through a ML approach (see Section 2) is generated. For each $\mathbf{Y}_n$, the conductivity field, $\mathbf{K}_n$, is reconstructed in the study area according to the *CM* and *OC* model.

(2) The forward groundwater flow model is solved for all conductivity fields $\mathbf{K}_n$ upon setting a flow rate equal to $Q^{\min}$ in all pumping wells.

(3) As a result of step (2), Region A is identified. It includes the number of N_A realizations of **K** (and of **Y**) for which the *SF* is always detected.

(4) The forward groundwater flow model is solved for all conductivity fields $\mathbf{K}_n$ not included in Region A upon setting a flow rate equal to $Q^{\max}$ in all pumping wells.

(5) As a result of step (4), Region C is identified. It includes the number of N_C realizations of **K** (and of **Y**) for which the *SF* is never detected.

(6) As a result of steps (3) and (5), Region B is identified, which includes $N_B = N - N_A - N_C$ realizations of **K**.

(7) Entries of vector **Q** are considered independent and identically distributed (iid) random variables characterized by a uniform distribution within the support [$Q^{\min}$, $Q^{\max}$] and are sampled M times through a Latin Hypercube Sampling strategy.

(8) Groundwater flow simulations are run upon setting $\mathbf{Q} = \mathbf{Q}_m$ (m = 1,…, M) for all N_B realizations of **K** to evaluate the relative frequency corresponding to the number of realizations where (1) is satisfied.

This procedure requires performing 2N (Steps 2 and 4) + $N_B \times M$ (step 8) runs of the forward groundwater flow model for each conceptual model of the system. It can be remarked that the values of N and M need to be sufficiently high to ensure stability in the computation of the target probabilities. In this context, note that relying on the full groundwater model set-up described in Section 2 to simulate hydraulic heads at the spring locations poses a significant challenge in terms of computational effort. For this reason, the target system response is evaluated upon relying on a surrogate (or reduced-order) model. For the purpose of our study, a surrogate model based on the generalized Polynomial Chaos Expansion (gPCE; e.g., Ghanem and Spanos, 1991; Xiu and Karniadakis, 2002; Le Maître and Knio, 2010) is considered, the presented probabilistic risk assessment methodology being fully compatible with other choices of model reduction techniques. Details about the methodology employed to obtain the surrogate model approximation are illustrated in Appendix B.

The framework of analysis is exemplified in Section 4 upon considering N_w = 5 pumping wells located in the area with the highest spring density. The identifiers associated with these wells are (from North to South): Arzago, Misano, Capralba, Sergnano, and Spino. The hydraulic head constraint expressed by (1) is applied to N_s = 34 natural springs located in the proximity of these wells. The location of the pumping wells and of the springs is depicted in Fig. 1b. The flow rate Q_w (w = 1, ..., 5) of each well is allowed to vary between $Q^{\min} = 0$ and $Q^{\max} = 0.9$ m^3/sec. This range of values has been selected upon considering that the total amount of water withdrawn from these wells in the calibrated models (see Section 4 and Appendix A) is 1.18 m^3/s (corresponding to 3.72×10^7 m^3/year) and with the aim of including in the analysis also scenarios mimicking a significant increase of groundwater withdrawal from the aquifer. A minimum flow rate $Q_s^{\min}$ = 0.097 m^3/s is set at each spring. This value ensures a minimum value for the total spring flow rate equal to 3.31 m^3/s. The latter corresponds to a decrease of 25 % with respect to the value employed in the calibrated models, i.e., 4.42 m^3/s (see Section 4 and Appendix A).

4. Results and discussion

Values of ML estimates ($\boldsymbol{\mu}$) of facies log-conductivities as well as a the posterior covariance matrix ($\boldsymbol{\Sigma}$) of the corresponding estimation error are listed in Table 2 for the two conceptual models considered. Figure 4 compares the prior (Uniform) probability density functions (see Appendix A, Table A.1), *pdf*, of each parameter against their (marginal, Gaussian) posterior counterparts stemming from model calibration. ML conductivity estimates are consistent with the nature of the geomaterials with which they are associated, lowest and largest values being referred to clay (Facies 1) and gravel and fractured conglomerate (Facies 2 and 3), respectively. The uncertainty related to these estimates (as quantified in terms of the diagonal entries of $\mathbf{\Sigma}$) is (at least) one order of magnitude smaller than the (prior) uncertainty corresponding to each parameter (as quantified through the variance of the prior *pdf*), in line with the ability of hydraulic head data to increase our level of knowledge of hydraulic parameters of the geomaterials contributing to internal make-up of the system.

The spatial distribution of hydraulic heads computed with the calibrated *CM* and *OC* models is depicted in Fig. 1b. The main flow direction is from North to South, the hydraulic gradient decreasing mildly along this direction, with a mean value of approximately 3.7‰. One can note that both calibrated models yield essentially the same overall distribution of hydraulic heads, an observation which is also supported by the results shown in Appendix A and related to the ability of the calibrated models to reproduce the observed heads (see scatterplot in Figure A.2) as well as the mean annual total discharge at the natural springs (see Appendix A).

Following the workflow described in Section 3.2 and in Fig. 3, the probabilities $P[Y_A]$, $P[Y_C]$, and $P[Y_B] = 1 - P[Y_A] - P[Y_C]$ are computed. This is accomplished upon relying on a sample of $N = 10^4$ realizations of $\mathbf{K}$ which enables one to obtain stable evaluation of the quantities of interest (details not shown). Values $P[Y_A]$ = 38.4%, $P[Y_B]$ = 46.5%, and $P[Y_C]$ = 15.1% for *CM*; and $P[Y_A]$ = 33.7%, $P[Y_B]$ = 32.4%, and $P[Y_C]$ = 33.9% for *OC* are obtained in our scenarios. The resulting Regions A, B and C are depicted in Fig. 5 across the considered parameter spaces for *CM* (Fig 5a) and *OC* (Fig. 5b). One can note that the two modeling approaches yield similar values of $P[Y_A]$, i.e., the probability that a scenario falls within the region where the desired constraints cannot be satisfied. Conversely, the choice of the conceptual model strongly affects $P[Y_C]$ (and therefore $P[Y_B]$), a higher probability to be in Region C (where *SF* is never detected) being observed for *OC* than for *CM*. This result is related to the observation that the uncertainty in the conductivity field may have a different impact on the variability of hydraulic heads depending on the conceptual model adopted. In this sense, it is noted that local sharp changes of hydraulic conductivity can occur in *CM*, while *OC* leads to a smoother spatial variation of conductivity. Therefore, *CM* is (in general) characterized by spatial variations of the hydraulic gradient that are larger than the ones observed in *OC*, yielding a higher probability in *CM* than in *OC* that a given conductivity realization be associated with Region C. In this context, the results related to the *CM* model can be viewed as more conservative than those linked to *OC* for the purpose of the risk analysis here considered.

The overall probability of system failure, $P[SF]$, evaluated according to (9) and considering M = 10^5 random realizations of well flow rates, $\mathbf{Q}_m$ (m = 1,…, M), is depicted in Fig. 6 as a function of the total (normalized) volume of water withdrawn from the aquifer per unit time by the system of pumping wells, $Q_T^* = \sum_{w=1}^{N_w} Q_w / Q_{\max}$. Relying on $M = 10^5$ enable one to investigate the system behavior for a sufficiently high number of combinations of flow rates at the five investigated wells. The variability of $P[SF]$ associated with a given value of Q_T^* in Fig. 6 is related to the way Q_T^* is partitioned amongst the wells and its analysis enables one to quantify the influence of such a partitioning on $P[SF]$. It is noted that the impact of the flow rate distribution amongst the wells is larger in *CM* than in *OC*. For each modeling approach, the lower bound of the cloud of points in Fig. 6 leads to identifying the best trade-off between the need to maximize the benefit associated with water withdrawal from the aquifer while minimizing $P[SF]$. As such, it can be identified as a Pareto front, collecting the solutions for which an improvement to a given objective (corresponding to maximizing Q_T^* in our example) is not possible without a reduction in the possibility of achieving another objective, i.e., here represented by the minimization of $P[SF]$ (Deb et al., 2002). These results are based on specific definitions of system failure, design variables, scenarios and sources of uncertainty. In this context, the evaluation of the probability of system failure provides a quantitative basis which one can then envision to include as a tool in a decision support system in the framework of groundwater resources management and protection. While costs associated with alternative exploitation strategies are not explicitly considered in this study, these can be accounted for in a cost-benefit analysis for which our risk assessment provides input. All of these elements underpin the results of probabilistic risk analyses and would benefit from a continuous update and refinement stemming from a participatory process and feedback with policy makers, local authorities, and stakeholders.

Figure 7a depicts the total normalized flow rate as a function of $P[SF]$ for some selected points at the Pareto front. Corresponding distribution of optimal normalized flow rates, $Q_w^* = Q_w / Q^{\max}$, for each of the five wells considered in the analysis are depicted in Figs. 8b and 8c for *CM* and *OC*, respectively. A conceptualization of the subsurface system based on *OC* leads to the possibility of extracting an increased water volume from the aquifer with respect to *CM* for a given value of $P[SF]$. This is consistent with the observation that $P[Y_C]$ is smaller for *CM* than for *OC*, as noted above. For both modeling approaches it can be noted that the optimal total flow rate increases almost linearly with $P[SF]$ (see Fig. 7a). Otherwise, a non-linear trend is observed when plotting the values of the normalized optimal well rates at each well versus $P[SF]$ (Figs. 7b-c), possibly due to local effects. For example, the rate of increase of optimal pumping rate with $P[SF]$ at the Misano well for *CM* is very low in the interval $0.45 < P[SF] < 0.65$ and sharply increases for $P[SF] > 0.70$ (see Fig. 7b). When considering the *OC* model, the optimum values of the pumping rates at the Spino and Arzago wells are close to the upper bound of the assigned range of variability for e.g. $0.55 < P[SF] < 0.65$. This result is associated with the values of hydraulic head thresholds that have been imposed at the springs closest to these wells.

The analyses illustrated above do not enable one to identify the most vulnerable spring of the system because of the way *SF* is defined in our application example, i.e., the depletion of at least one spring. In the context of environmental applications, such a choice is grounded on the interest in considering the most conservative scenario and guaranteeing a minimum flow rate for each spring in the system, as compatible with environmental requirements. Otherwise, one could also be interested in assessing which amongst the springs in the system would be associated with the highest risk of depletion, depending on the adopted pumping scheme. This issue is addressed upon evaluating the relative frequency of spring depletion considering various pumping schemes. The probability of failure for the j-th spring ($P[SpF_j]$; j = 1, …, 34) is evaluated as the number of times the constraint (1) is not satisfied across the collection of $N = 10^4$ realizations of $\mathbf{K}$. As an example of the results one can obtain, the case at the Pareto front associated with Fig. 7b-c and $P[SF] = 0.45$ is considered. The (normalized) flow rate for each well in the system (one well at a time) is then varied between 0 and 1, while fixing the remaining four extracted rates at their optimal values (represented in Fig. 7b-c). Results of this analysis are depicted in Figs. 8 and 9 for *CM* and *OC*, respectively. In order to streamline the analysis, the 34 springs in the area are organized into 5 groups, according the closest well. The group of springs associated with the well whose flow rate is varied in this analysis is identified with a red bracket in the various panels of Figs. 8 and 9. As expected, for both modeling approaches it is observed that increasing the flow rate at a given well mainly affects $P[SpF_j]$ at the subset of springs located in its proximity (and demarcated by the red bracket). In particular, the Spino well can only affect the value of $P[SpF_j]$ at the corresponding group of springs for both *CM* and *OC* (see Figs. 8e and 9e). This finding is consistent with the observation that this well is quite isolated with respect to the others (see Fig. 1b). Note that each of the springs within a given group is characterized by a unique behavior in terms of $P[SpF_j]$, which is associated with the risk of depletion for increasing pumping rates of the closest well. Similar results have been obtained for $P[SF] > 0.45$ (not shown). For completeness, a statistical analysis of hydraulic head evaluated at all spring locations corresponding to the pumping scheme of Fig. 7b-c and $P[SF] = 0.45$ is provided as Supplementary Data.

5. Conclusions

Our study provides methodological advancements by proposing a novel approach for Probabilistic Risk Assessment (PRA) targeting reduction of the flow rate at natural springs due to excessive aquifer exploitation for supply or productive use. The approach and ensuing operational workflow are exemplified considering a three-dimensional, large scale aquifer system whose characterization is fraught by elements of uncertainty related to the possibility of representing the subsurface through diverse conceptual geological models, each associated with uncertain hydraulic parameters. The level of knowledge of the latter is conditioned to available hydraulic head information through a Maximum Likelihood inverse modeling approach. Our analysis explicitly includes the impact of model and associated parameter uncertainty on the evaluation of the probability of system failure. The latter is quantified through the constrain that hydraulic head of a target set of active springs does not fall below a given threshold value as a consequence of groundwater pumping.

The application of the approach we present to the investigated field site leads to the following major conclusions.

1. The choice of the conceptual model employed to characterize the internal geological makeup of the groundwater system strongly affects probability of system failure. While the scenario corresponding to conceptual geological model based on a composite medium (*CM*) approach yields locally sharp changes of hydraulic conductivity (and therefore of hydraulic head gradients), the setting corresponding to an overlapping continua (*OC*) approach leads to smoother spatial variations of these quantities. As a consequence, uncertainties associated with the ensuing conductivity fields, even as constrained through model calibration, has a different impact on the variability of hydraulic heads depending on the conceptual model adopted.
2. Our methodology enables one to include uncertainty in model parameters which is constrained by available hydraulic head information through a Maximum Likelihood inverse modeling approach. This element provides a marked interconnection between the processes of model calibration and the use of a given model for predictions of the system response due to possible changes in the forcing terms.

3. For a given groundwater withdrawal, probability of system failure is smaller for the overlapping continua than for the composite medium approach. As such, the latter scenario can be viewed as more conservative than its counterpart based on the overlapping continua concept for the purpose of the probabilistic analysis here considered.
4. Our operational workflow conducive to the Probabilistic Risk Assessment of natural springs under uncertainty makes effective use of a combination of Fault Tree Analysis, inverse modeling of a large scale groundwater flow system, development of a surrogate groundwater flow model, and uncertainty quantification to evaluate the probability that the functioning of the system considered attains a critical state. The proposed methodology allows assessing the best compromise between two conflicting objectives, corresponding to (*i*) the minimization of probability of system failure and (*ii*) the possibility to guarantee significant groundwater extraction rates, with the aim of identifying the optimal total flow rate as well as its optimal distribution amongst operating pumping wells. The structure of the methodology renders it amenable to be effectively included in a decision support system for groundwater resources management and exploitation.

6. Appendix

Appendix A – Model calibration

For each conceptual model, estimates of facies log-conductivities, $Y_i = log\ k_i$ (i = 1, ..., N_p), and of the leakage coefficient, l_d, have been obtained through an inverse modeling approach upon relying on a Maximum Likelihood (ML) framework (see e.g., Carrera and Neumann, 1986; Poeter and Hill, 1997; Tarantola, 2005; Carrera et al., 2005; Chavent, 2010).

The level of knowledge of the uncertain hydraulic parameters is conditioned to available hydraulic head information through a Maximum Likelihood inverse modeling approach. Let N_p and N_h be the number of unknown model parameters and hydraulic head measurements, respectively. The vector of unknown model parameters, $\mathbf{p} = \left[p_1, p_2, ..., p_{N_p} \right]$, the vector of hydraulic head measurements, $\mathbf{h}^* = \left[h_1^*, h_2^*, ..., h_{N_h}^* \right]$, the vector of model predictions, $\hat{\mathbf{h}} = \left[\hat{h}_1, \hat{h}_2, ..., \hat{h}_{N_h} \right]$, and the prior covariance matrix of the head measurement errors, $\mathbf{C}_h$, are then introduced. As commonly assumed (e.g., Carrera and Neuman, 1986), errors h_i^* are considered to be uncorrelated. This renders $\mathbf{C}_h = \sigma_h^2 \mathbf{V}_h$ diagonal with the nonzero terms equal to the head observation error variance, σ_h^2 .

The Maximum Likelihood (ML) estimate, $\hat{\mathbf{p}}$, of $\mathbf{p}$ is obtained through minimization of the negative log likelihood criterion (e.g., Carrera and Neumann, 1986; Bentley, 1993; Poeter and Hill, 1997; Tarantola, 2005; Carrera et al., 2005; Chavent, 2010)

$$NLL = \sum_{i}^{N_h} \frac{J_i}{\sigma_h^2} + \ln |\mathbf{C}_h| + N_h \ln(2\pi) \tag{10}$$

with respect to **p**. The quantity J_i in Eq. (10) is defined as the squared difference between measured and predicted hydraulic heads

$$J_i = \left(h_i^* - \hat{h}_i \right)^2 . \tag{11}$$

Considering σ_h^2 as a constant, minimizing *NLL* (for fixed N_h) is tantamount to minimizing the least square criterion

$$J = \sum_{i=1}^{N_h} \left(h_i^* - \hat{h}_i \right)^2 \tag{12}$$

Minimization of Eq. (12) is performed upon relying on the iterative Levenberg-Marquardt algorithm implemented in the public domain code PEST (Doerthy, 2018). Then, the ML estimate of σ_h^2 is given by

$$\hat{\sigma}_h^2 = \frac{J_{\min}}{N_h} \tag{13}$$

where $J_{\min}$ is the minimum of J.

The posterior estimation error covariance matrix, $\mathbf{\Sigma}$, is a measure of the quality of parameter estimates conditioned to available hydraulic head information and is estimated as (Carrera and Neuman, 1986)

$$\mathbf{\Sigma} = \hat{\sigma}_h^2 \left[\mathbf{S}^T \mathbf{V}_h^{-1} \mathbf{S} \right]^{-1}. \tag{14}$$

Here, $\mathbf{S}$ is the Jacobian (sensitivity) matrix, whose components are $\partial h_r / \partial p_i$ with (r = 1,…, N_h; and i = 1, …, N_p).

As calibration data, we consider yearly-averaged hydraulic heads collected at 35 observation wells during year 2015 and mean annual total discharge monitored at the springs, Q_{sp}. Location of monitoring wells and springs is depicted in Fig. 1b. Details about available data are offered in Bianchi Janetti et al. (2019). Lower and upper bounds assigned to Y_i prior to model calibrations are based on typical values of hydraulic conductivities characterizing each of the identified geomaterials (see Table A.1).

Calibration of model parameters has been performed using the following iterative procedure:

i) Facies log-conductivity values, Y_i, are estimated considering the available hydraulic head measurements and a first tentative value for the leakage coefficient, l_d;

ii) An estimate of l_d is obtained by considering available data about Q_{sp} while setting hydraulic conductivities at the optimal values obtained at step (*i*);

iii) Values of Y_i are subject to a further estimation process while setting l_d at the value resulting from step (*ii*) and are then compared against the values obtained at step (*i*).

Convergence of the procedure requires only a few iterations, leading to optimal values of Y_i and l_d obtained on the basis of both hydraulic head and spring flow rate measurements. Estimated values of l_d are 1.21×10^{-6} s^{-1} and 1.30×10^{-6} s^{-1} for *CM* and *OC*, respectively.

Figure A.2 depicts scatterplots of simulated versus observed hydraulic heads at the available monitoring stations for *CM* (Fig. A.1a) and *OC* (Fig. A.1b). These results suggest that both calibrated models can accurately reproduce available hydraulic head observations at the site. Groundwater levels obtained for each spring location in the two calibrated models are depicted in Figure A.2.

Appendix B – Surrogate model

The uncertain model inputs are here associated with (*a*) flow rates Q_w (with $w = N_w$) related to the pumping wells considered in the analysis and (*b*) facies log-conductivities (Y_i, with $i = n_f$) . Uncertain parameters are collected in a vector $\mathbf{p}$ = [$\mathbf{Q}$, $\mathbf{Y}$] of dimension $D = N_w + N_p$. For the purpose of evaluating the surrogate model, we consider the entries of $\mathbf{Q}$ and $\mathbf{Y}$ as independent and identically distributed (iid) random variables, each characterized by a uniform density. The (random) parameter space across which the full system model is evaluated and the surrogate model is constructed is then defined as $\mathbf{\Gamma} = \left[\mathbf{p}^{\min}, \mathbf{p}^{\max}\right]$, $\mathbf{p}^{\min}$ and $\mathbf{p}^{\max}$ denoting vectors containing lower and upper bounds of parameter variability intervals, respectively (see Table A.1). We set $Q_w^{\min}$ = 0 and $Q_w^{\max}$ = 0.9 m^3 s^{-1} for all wells, according to the scenarios described in Section 3.2. The choice of $Y_i^{\min}$ and $Y_i^{\max}$ is based on typical hydraulic characteristics of each of the identified geomaterials (see Fig. 4 and Table A.1). As stated in Section 3.2, our surrogate (or reduced-order) model relies on the generalized Polynomial Chaos Expansion (gPCE; e.g., Ghanem and Spanos, 1991; Xiu and Karniadakis, 2002; Le Maître and

Knio, 2010). We then approximate $h_j\left(\mathbf{Q},\mathbf{Y}\right)$ in Eq. (1) through a linear combination of multivariate orthonormal Legendre polynomials, i.e., $\psi_{\boldsymbol{x}}(\boldsymbol{p})$, as

$$
\begin{aligned}
&f(\boldsymbol{p}) \cong f_0 + \sum_{i=1}^{D} \sum_{\boldsymbol{x}\in\Im_i} \beta_{\boldsymbol{x}} \psi_{\boldsymbol{x}}(\boldsymbol{p}) + \sum_{i=1}^{D} \sum_{j=1}^{D} \sum_{\boldsymbol{x}\in\Im_{i,j}} \beta_{\boldsymbol{x}} \psi_{\boldsymbol{x}}(\boldsymbol{p}) + ...; \\
&\psi_{\boldsymbol{x}}(\boldsymbol{p}) = \prod_{i=1}^{D} \psi_{i,x_i}(p_i); \quad \beta_{\boldsymbol{x}} = \int_{\Gamma} f(\boldsymbol{p}) \psi_{\boldsymbol{x}}(\boldsymbol{p}) \rho_{\Gamma_{\boldsymbol{p}}}\, d\boldsymbol{p},
\end{aligned}
\tag{15}
$$

where $\boldsymbol{x} = \left\{x_1,...,x_M\right\} \in \mathrm{N}^M$ is a multi-index expressing the degree of each univariate polynomial, $\psi_{i,x_i}(p_i)$; $\beta_{\boldsymbol{x}}$ are the gPCE coefficients; $\rho_{\Gamma_{\boldsymbol{p}}}$ denotes the *pdf* of **p**; $\Im_i$ and $\Im_{i,j}$ include all indices such that only the *i*-th component does not vanish or only the *i*-th and *j*-th components are not zero, respectively, and so on. Evaluating coefficients $\beta_{\boldsymbol{x}}$ in Eq. (15) entails resorting to a regression-based method (Sudret, 2008). The latter is based on (*a*) the evaluation of the full model and its gPCE approximation at a number of points in the parameter space and (*b*) the minimization of the sum of the square of the differences between the exact and the approximated solutions. Here, accurate results have been obtained truncating the gPCE at order 3, requiring N_t = 1115 and 720 full model runs for *CM* and *OC*, respectively (due to the different number of input parameters) which are performed using a quasi-Monte Carlo sampling technique (see e.g., Feil et al., 2009; Fajraoui et al., 2012; Maina and Guadagnini, 2018). The ability of a gPCE of a given order to approximate hydraulic heads at the target points (i.e., locations corresponding to the springs) is assessed upon considering the full model solutions evaluated at N_V = 100 sets of parameter values, randomly selected in the parameter space and not employed for the assessment of the gPCE. Figure B.1 depicts scatterplots of $h_{gPCE,j,k}$ versus $h_{j,k}$ computed for the two conceptual models considered at all target points *j* (corresponding with the 34 spring locations introduced in Section 3.2) for all N_V sets. This figure clearly shows a good agreement between $h_{j,k}$ and $h_{gPCE,j,k}$. We also computed a mean absolute relative error ($MARE_j$) between the full model and the gPCE approximation for each spring location, i.e.,

$$MARE_j = \frac{1}{N_V}\sum_{k=1}^{N_V}\frac{\left|h_{j,k} - h_{gPCE,j,k}\right|}{h_{j,k}} \qquad j = 1,....,N_s \tag{16}$$

Average values of this metric, evaluated across the set of N_s spring locations, are 0.017 % and 0.035 % for *CM* and *OC*, respectively. These results suggest that the considered surrogate models enables us to capture with high fidelity the full model results needed for the purpose of our analysis.

Acknowledgements

The authors would like to thank the EU and MIUR for funding, in the frame of the collaborative international Consortium (WE-NEED) financed under the ERA-NET WaterWorks2014 Cofunded Call. This ERA-NET is an integral part of the 2015 Joint Activities developed by the Water Challenges for a Changing World Joint Programme Initiative (Water JPI).

References

Amanambua, A.C., Obarein, O.A., Mossa, J., Li., L., Ayeni, S.S., Balogun, O., Oyebamiji, A., Ochege, F.U., 2020. Groundwater system and climate change: Present status and future considerations. J. Hydrol. 589, 125163. https://doi.org/10.1016/j.jhydrol.2020.125163.

Bedford, T., Cooke R., 2003. Probabilistic Risk Analysis: Foundations and Methods. Cambridge Univ. Press. New York.

Bianchi Janetti, E., Guadagnini, L., Riva, M., Guadagnini, A., 2019. Global sensitivity analyses of multiple conceptual models with uncertain parameters driving groundwater flow in a regional-scale sedimentary aquifer. J. Hydrol. 574, 544-556. https://doi.org/10.1016/j.jhydrol.2019.04.035.

Bolster, D., Barahona, M., Dentz, M., Fernàndez-Garcia, D., Sanchez-Vila, X., Trinchero, P., Valhondo C., Tartakovsky, D. M., 2009. Probabilistic Risk Analysis of Groundwater Remediation Strategies, Water Resour. Res., 45, W06413. https://doi.org/10.1029/2008WR007551.

Carrera, J., Neuman, S.P., 1986. Estimation of aquifer parameters under transient and steady state conditions:1. Maximum likelihood method incorporating prior information. Water Resour. Res. 22 (2), 199-210. https://doi.org/10.1029/WR022i002p00199.

Carrera, J., Alcolea, A., Medina, A., Hidalgo, J., Slooten, L.J., 2005. Inverse problem in hydrogeology. Hydrogeol. J. 13(1), 206-222. https://doi.org/10.1007/s10040-004-0404-7.

Castellazzi, P., Martel, R., Rivera, A., Huang, J., Pavlic, G., Calderhead, A.I., Chaussard, E., Garfias, J., Salas, J., 2016. Groundwater depletion in Central Mexico: Use of GRACE and InSAR to support water resources management. Water Resour. Res. 52 (8): 5985-6003. https://doi.org/10.1002/2015WR018211.

Chavent, G., 2010. Nonlinear least squares for inverse problems. Springer. ISBN 978-90-481-2785-6

Deb, K., Pratap, A., Agarwal, S., Meyarivan, T., 2002. A fast and elitist multiobjective genetic algorithm: NSGA-II. IEEE Trans. Evol. Comput. 6 (2), 182-197.

Doherty, J. 2018. PEST: Model independent parameter estimation, user manual. 7th ed. Watermark Numer. Computing, Corinda, Queensland.

Epting, J., Huggenberger, P., Radny, D., Hammes, F., Hollender, J., Page, R.M., Weber, S., Bänninger, D., Auckenthaler, A., 2018. Spatiotemporal scales of river-groundwater interaction-The role of local interaction processes and regional groundwater regimes. Sci. Total Environ. 618, 1224-1243. https://doi.org/10.1016/j.scitotenv.2017.09.219.

Fajraoui, N., Mara, T.A., Younes, A., Bouhlila, R., 2012. Reactive transport parameter estimation and global sensitivity analysis using sparse polynomial chaos expansion. Water Air Soil Poll. 223 (7), 4183-4197. https://doi.org/10.1007/s11270-012-1183-8.

Feil, B., Kucherenko, S., Shah, N., 2009. Comparison of Monte Carlo and Quasi Monte Carlo sampling methods in high dimensional model representation. In 2009 first international conference on advances in system simulation (pp. 12-17). New York, NY: IEEE. https://doi.org/10.1109/SIMUL.2009.34.

Fernàndez-Garcia, D., Bolster, D., Sanchez-Vila, X., Tartakowsky, D.M., 2012. A Bayesian approach to integrate temporal data into probabilistic risk analysis of monitored NAPL remediation. Adv. Water Res. 36, 108-120. https://doi.org/10.1016/j.advwatres.2011.07.001.

Filimonau, V., Barth, J.A.C., 2016. From global to local and vice versa: on the importance of the 'globalization' agenda in continental groundwater research and policy-making. Environ. Manag. 58 (3), 491-503. https://doi.org/10.1007/s00267-016-0722-2.

Ghanem, R.G., Spanos, P.D., 1991. Stochastic Finite Elements: A Spectral Approach, Springer, N. Y.

Gleeson, T., Wada, Y., Bierkens, M.F.P., van Beek, L.P.H. 2012. Water balance of global aquifers revealed by groundwater footprint. Nature 488, 197-200. http://dx.doi.org/10.1038/nature11295.

Guadagnini, L., Guadagnini, A., Tartakovsky, D.M., 2004. Probabilistic reconstruction of geologic facies. J. Hydrol. 294, 57-67. https://doi.org/10.1016/j.jhydrol.2004.02.007.

Harbaugh, A.W., 2005. MODFLOW-2005. The U.S. Geological Survey Modular Ground-Water Model - the Ground-Water Flow Process. U.S. Geological Survey Techniques and Methods 6-A16.

Henri, C.V., Fernàndez-Garcia, D., de Barros, F.P.J., 2015. Probabilistic human health risk assessment of degradation-related chemical mixtures in heterogeneous aquifers: Risk statistics, hot spots, and preferential channels. Water Resour. Res., 51. https://doi.org/10.1002/2014WR016717.

Jia, X., O'Connor, D., Hou, D., Jin, Y., Li, G., Zheng, C., Ok, Y.S., Tsang, D.C.W., Luo, J., 2019. Groundwater depletion and contamination: Spatial distribution of groundwater resources sustainability in China. Sci. Total Environ. 672, 551-562. https://doi.org/10.1016/j.scitotenv.2019.03.457.

Jia, X., Hou, D., Wang, L., O'Connor, D., Luo, J., 2020. The development of groundwater research in the past 40 years: A burgeoning trend in groundwater depletion and sustainable management. J. Hydrol. 587, 125006. https://doi.org/10.1016/j.jhydrol.2020.125006

Jurado, A., De Gaspari, F., Vilarrasa, V., Bolster, D., Sánchez-Vila, X., Fernàndez-Garcia, D., Tartakovsky, D.M., 2011. Probabilistic analysis of groundwater-related risks at subsurface excavation sites. Eng. Geol., 125, 35-44. https://doi.org/10.1016/j.enggeo.2011.10.015.

Kang, F.X., Jin, M.G., Qin, P.R., 2011. Sustainable yield of a karst aquifer system: a case study of Jinan springs in northern China. Hydrogeo. J. 19 (4), 851-863. https://doi.org/10.1007/s10040-011-0725-2.

Le Maître, O., Knio, O., 2010. Spectral methods for uncertainty quantification. Scientific Computation, Springer, Heidelberg, Germany. https://doi.org/10.1007/978-90-481-3520-2_1.

Liu, X.M., Hu, L.T., Sun, K.N., 2018. Analysis of spring flow change in the Jinan city under influences of recent human activities. Proc. IAHS 379, 263-268. https://doi.org/10.5194/piahs-379-263-2018.

Luo, Q., Yang, Y., Qian, J., Wang, X., Chang, X., Ma, L., Li, F., Wu, J., 2020. Spring protection and sustainable management of groundwater resources in a spring field. J. Hydrol. 582, 124498. https://doi.org/10.1016/j.jhydrol.2019.124498.

Maina, F.Z., Guadagnini, A., 2018. Uncertainty quantification and global sensitivity analysis of subsurface flow parameters to gravimetric variations during pumping tests in unconfined aquifers. Water Resour. Res. 54, 501-518. https://doi.org/10.1002/2017WR021655.

Obolewski, K., Strzelczak, A., Glińska-Lewczuk, K., Osadowski, Z., Astel, A., Timofte, C.M., 2016. Ecohydrological relationship between benthic communities and environmental conditions in the spring area. Environ. Eng. Manag. J. 15 (6), 1281-1291. https://doi.org/10.30638/eemj.2016.139.

Pedretti, D., Barahona-Palomo, M., Bolster, D., Fernàndez-Garcia, D., Sanchez-Vila, X., Tartakovsky, D. M., 2011. Probabilistic Analysis of Maintenance and Operation of Artificial Recharge Ponds, Adv. Water Res. https://doi.org/10.1016/j.advwatres.2011.07.008.

Poeter, E.P., Hill, M.C., 1997. Inverse models: A necessary next step in groundwater modeling. Ground Water 35(2), 250-260.

Rodak, C, Silliman S., 2012. Probabilistic risk analysis and fault trees: initial discussion of application to identification of risk at a wellhead. Adv Water Resour. 36, 133-145. https://doi.org/10.1016/j.advwatres.2011.02.005

Siirila-Woodburn, E. R., Fernàndez-Garcia, D., Sanchez-Vila, X., 2015. Improving the accuracy of risk prediction from particle-based breakthrough curves reconstructed with kernel density estimators, Water Resour. Res., 51. https://doi.org/10.1002/2014WR016394.

Sudret, B., 2008. Global sensitivity analysis using polynomial chaos expansion. Reliab. Eng. Syst. Safe. 93(7), 964-979. https://doi.org/10.1016/i.ress.2007.04.002.

Tarantola, A., 2005. Inverse Problem Theory and Methods for Model Parameter Estimation Siam. https://doi.org/10.1137/1.9780898717921

Tartakovsky, D.M., 2007. Probabilistic risk analysis in subsurface hydrology, Geophys. Res. Lett., 34, L05404. https://doi.org/10.1029/2007GL029245.

Tartakovsky, D.M., 2013. Assessment and management of risk in subsurface hydrology: A review and perspective, Adv. Water Res., 51, 247-260. http://dx.doi.org/10.1016/j.advwatres.2012.04.007

Xiu, D., Karniakidis, G.E., 2002. The Wiener-Askey polynomial chaos for stochastic differential equations. SIAM J. Sci. Comput. 24, 614-644. https://doi.org/10.1137/S1064827501387826.

Winter, C.L., Tartakovsky, D.M., Guadagnini, A., 2003. Moment differential equations for flow in highly heterogeneous porous media. Surv. Geophys. 24(1), 81-106.

Zhang, Z.X., Liu, Y., Zhang, F.X., Zhang, L.X., 2017. Study on dynamic relationship of spring water in Jinan spring area based on gray relational analysis. IOP Conf. Series: Earth Environ. Sci. 128, 012068. http://dx.doi.org/10.1088/1755-1315/128/1/012068

Tables

Table. 1. List of the n_f = 5 facies (or geomaterial classes) identified in the study area, together with their volumetric fraction.

M_i	Description	f_i (%)
1	Clay and silt	36.77
2	Gravel, sand and gravel	32.92
3	Fractured conglomerate	10.64
4	Compact conglomerate, sandstone	14.94
5	Fine and silty sand	4.73

Table 2. Statistical parameters of the multivariate normal distributions considered in the analysis.

Groundwater Model	**ML estimates**	**Estimation error covariance matrix**
CM	$\boldsymbol{\mu} = \left[-4.39, -1.67, -1.92\right]$	$\boldsymbol{\Sigma} = \begin{bmatrix} 1.62\times10^{-3} & -2.57\times10^{-3} & 4.90\times10^{-3} \\ \cdots & 3.63\times10^{-2} & -1.40\times10^{-2} \\ \cdots & \cdots & 2.65\times10^{-2} \end{bmatrix}$
OC	$\boldsymbol{\mu} = \left[-1.74, -2.00\right]$	$\boldsymbol{\Sigma} = \begin{bmatrix} 2.60\times10^{-2} & 2.07\times10^{-2} \\ \cdots & 6.07\times10^{-2} \end{bmatrix}$

Appendix

Table A.1. Selected uncertain model inputs and associated intervals of variability, as defined by their lower (min) and upper (max) boundaries.

Parameter	Description	Min	Max
p_w (m^3/s) with w=1,…,5	Pumping rate at well w, Q_w	0	0.9
$Log\ p_6$ (m/s)	Log-conductivity of facies 1, Y_1	-5.5	-3.5
$Log\ p_7$ (m/s)	Log-conductivity of facies 2, Y_2	-3	-1
$Log\ p_8$ (m/s)	Log-conductivity of facies 3, Y_3	-2.5	-0.5

Figures

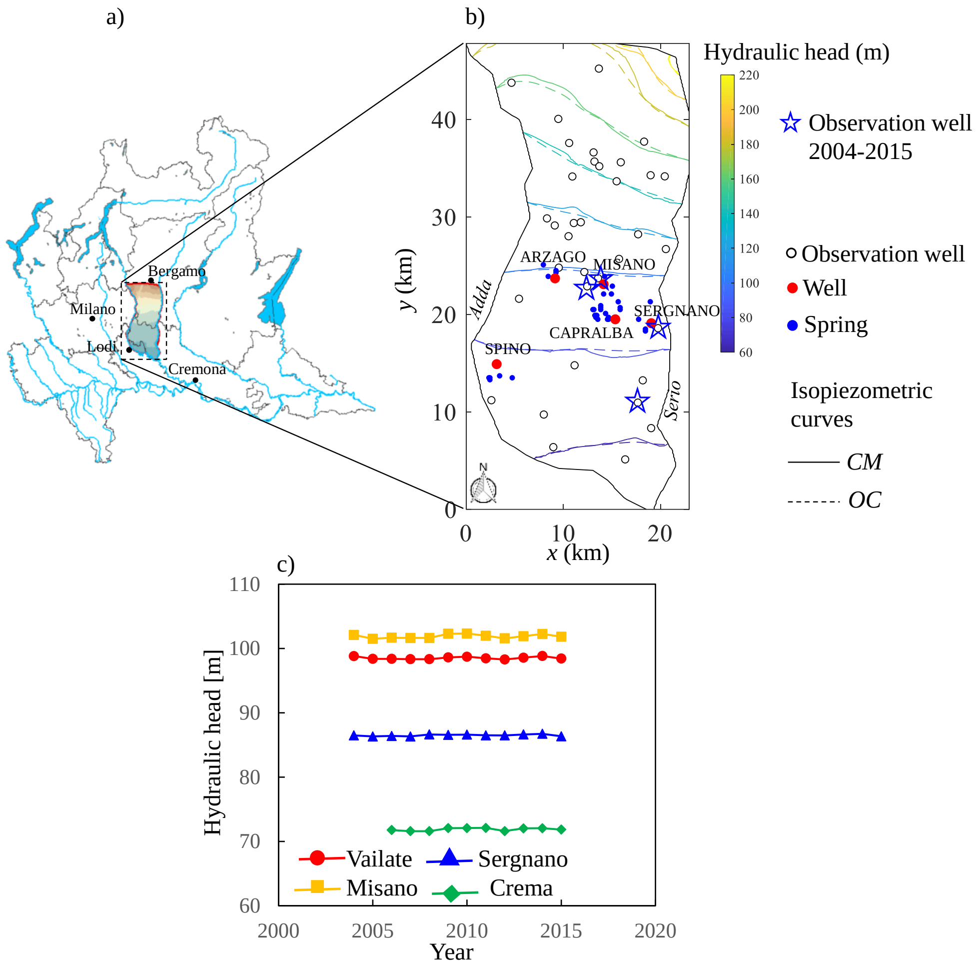

Figure 1. Location of (a) the study area (shaded zone) within the Po Plain (Northern Italy), (b) springs, pumping and observation wells considered in the analysis; hydraulic head distributions of the calibrated models are also shown, continuous and dashed curves being associated with the *Composite Medium* (*CM*) and the *Overlapping Continua* (*OC*) conceptual model, respectively; (c) yearly-averaged hydraulic head (years 2004 to 2015) at four observation wells (Vailate, Sergnano, Misano, and Crema) used in the model calibration process (locations of these observation wells within the study area (b) are identified with stars).

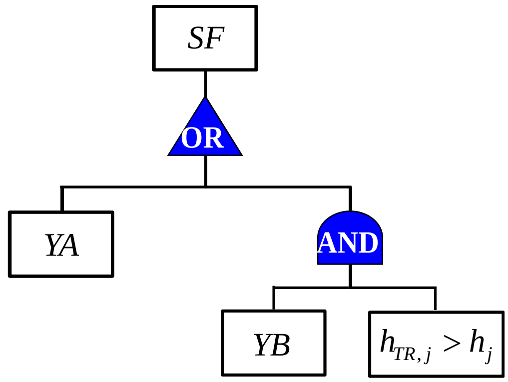

Figure 2. Fault tree leading to system failure (*SF*).

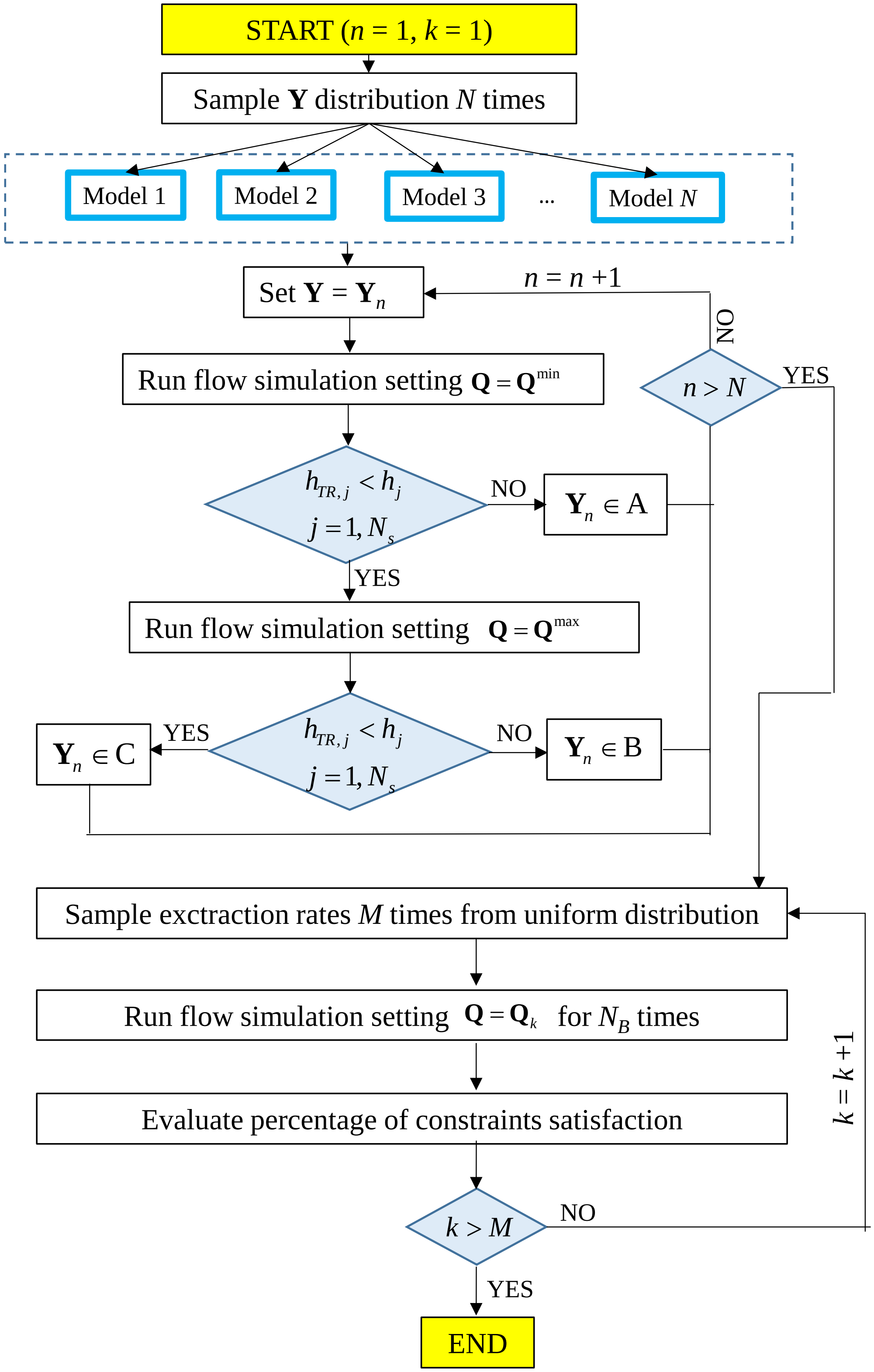

Figure 3. Workflow of the proposed methodology.

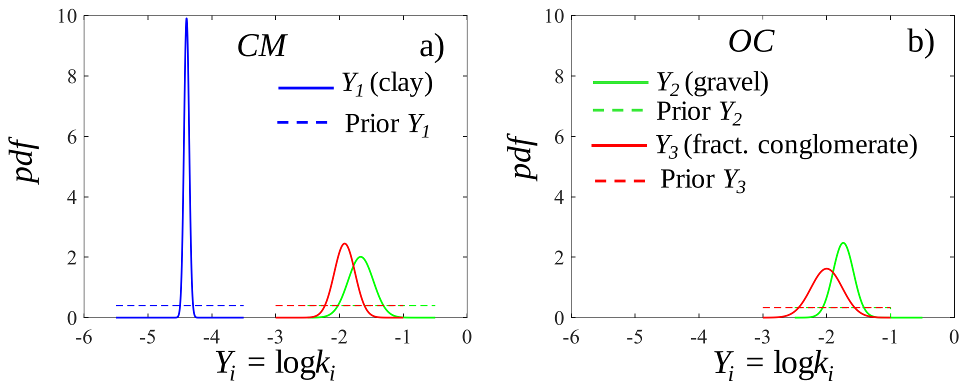

Figure 4. Marginal prior (dashed) and posterior (solid) *pdf* of facies log-conductivities for the (a) *Composite Medium* (*CM*) and (b) *Overlapping Continua* (*OC*) conceptual modeling approaches.

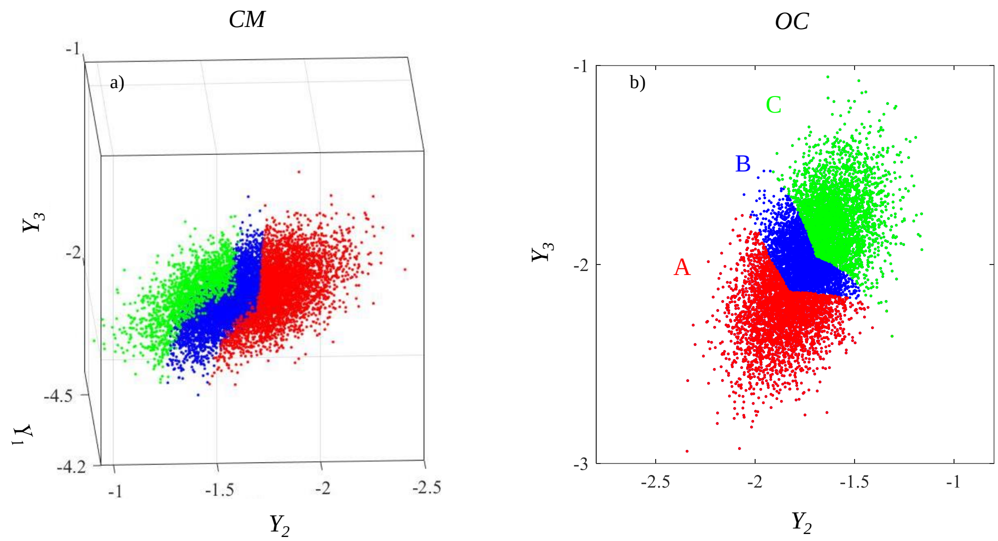

Figure 5. Identification of Region A (red), B (blue), and C (green) across the parameter space for the (a) *Composite Medium* (*CM*) and (b) *Overlapping Continua* (*OC*) conceptual modeling approaches.

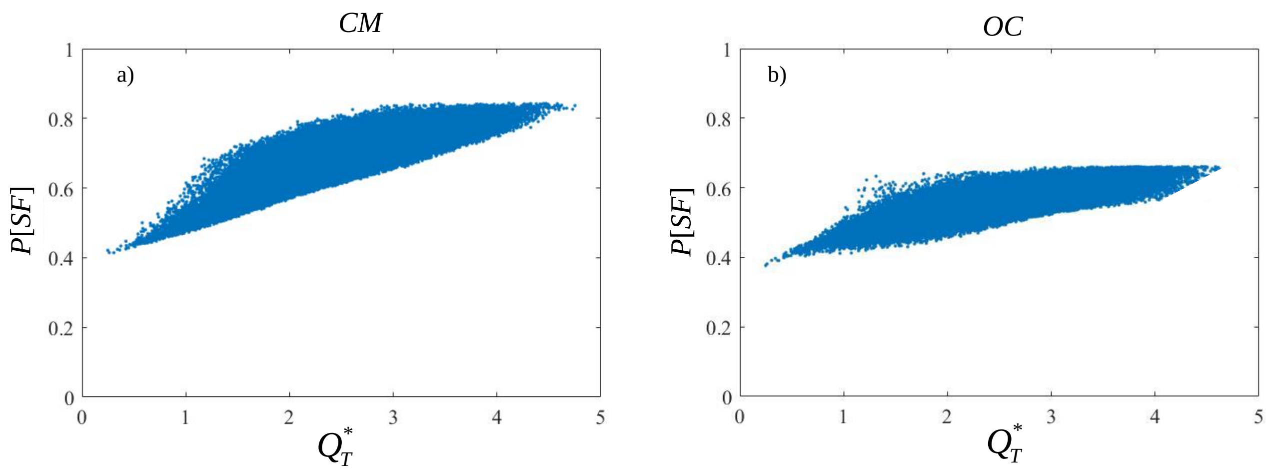

Figure 6. Probability of system failure ($P[SF]$) as a function of the total (normalized) rate extracted from the aquifer for the (a) *Composite Medium* (*CM*) and (b) *Overlapping Continua* (*OC*) conceptual modeling approaches.

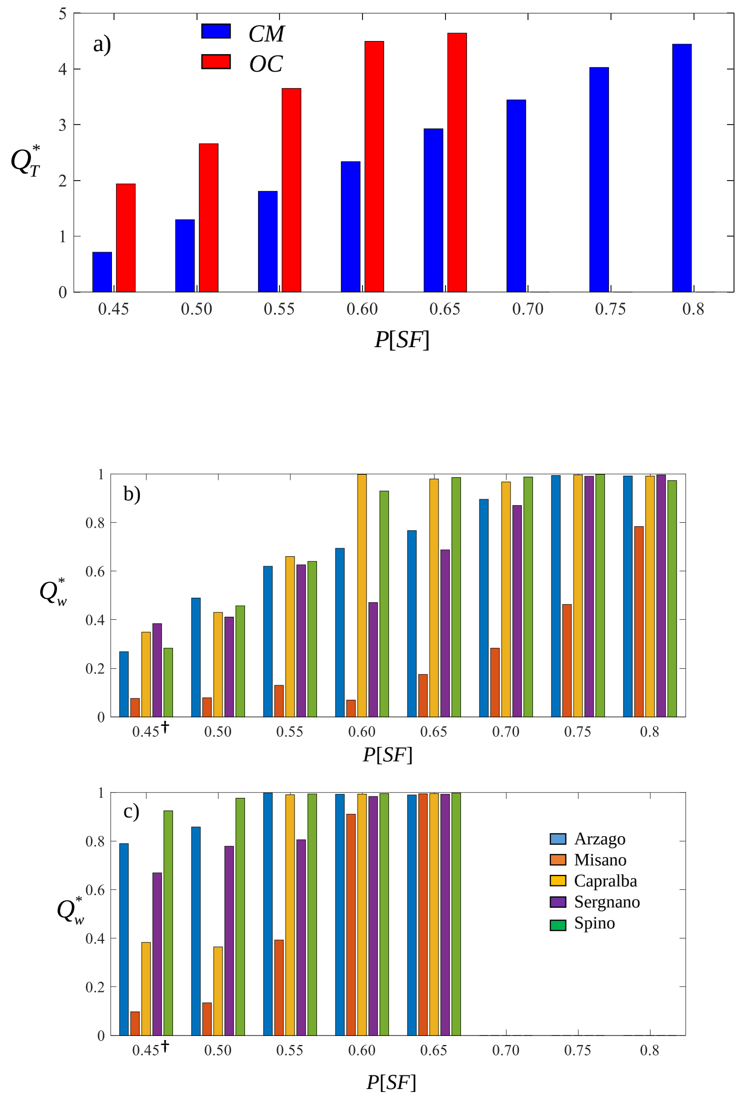

Figure 7. (a) Total flow rate versus $P[SF]$ for some selected points at the Pareto front of Fig. 7 for the *Composite Medium* (*CM*) and *Overlapping Continua* (*OC*) modeling approaches; and corresponding optimal normalized flow rate computed for each pumping well for (b) *CM* and (c) *OC*. The symbol † denotes the set of flow rates considered for the analysis shown in Figs. 8 and 9.

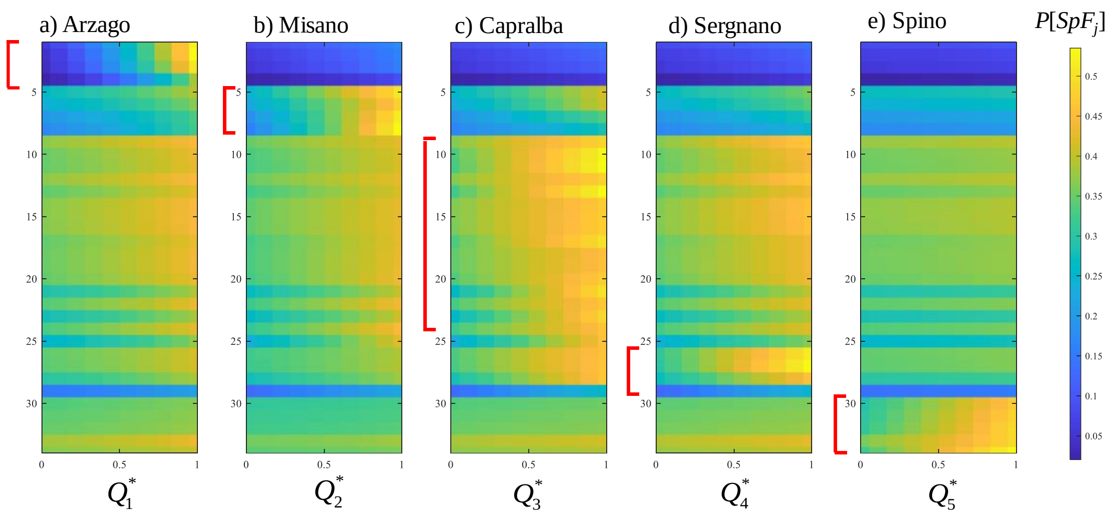

Figure 8. Probability that system failure takes places at the j-th spring ($P[SpF_j]$; j = 1, …, 34) evaluated upon varying the (normalized) flow rate at a single well Q_w^* (with w = 1 in (a), 2 in (b), 3 in (c), 4 in (d) and 5 in (e)), while keeping the remaining four extracted rates at their optimal values (represented in Fig. 7b-c and corresponding to $P[SF]$ = 0.45). Brackets identify the group of springs closest to the well whose flow rate is varied. Results are associated with the *Composite Medium* (*CM*) modeling approach.

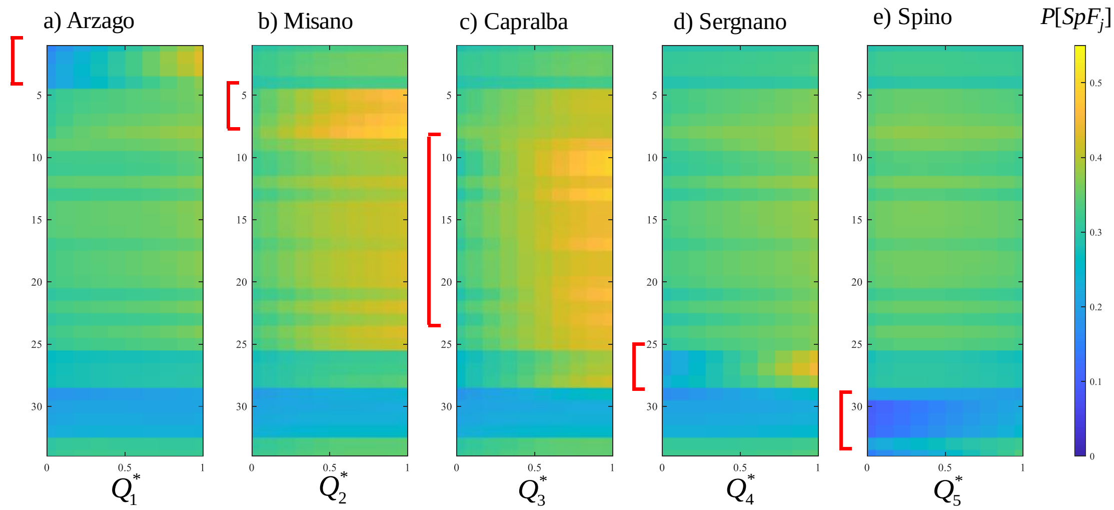

Figure 9. Probability that system failure takes places at the j-th spring ($P[SpF_j]$; j = 1, …, 34) evaluated upon varying the (normalized) flow rate at a single well Q_w^* (with w = 1 in (a), 2 in (b), 3 in (c), 4 in (d) and 5 in (e)), while keeping the remaining four extracted rates at their optimal values (represented in Fig. 7b-c and corresponding to $P[SF]$ = 0.45). Results are associated with the *Overlapping Continua* (*OC*) modeling approach.

Appendix A

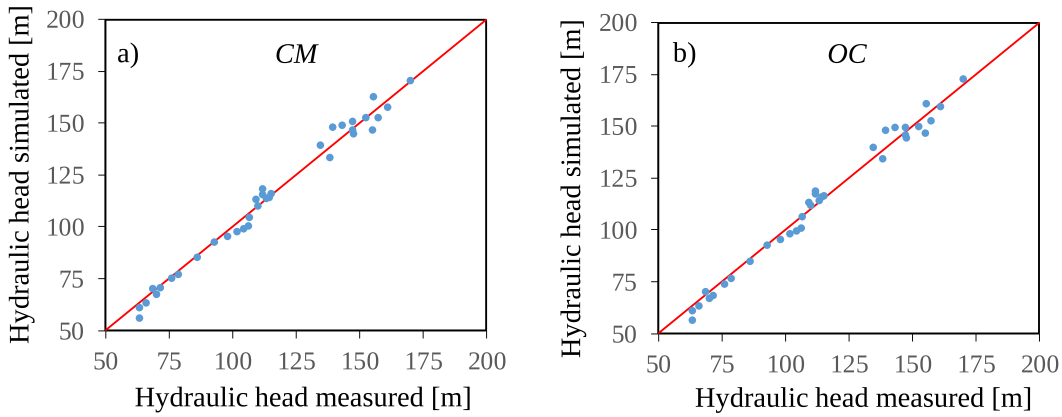

Figure A.1. Simulated versus measured hydraulic heads at observation well locations for the (a) *Composite Medium* (*CM*) and (b) *Overlapping Continua* (*OC*) conceptual modeling approaches.

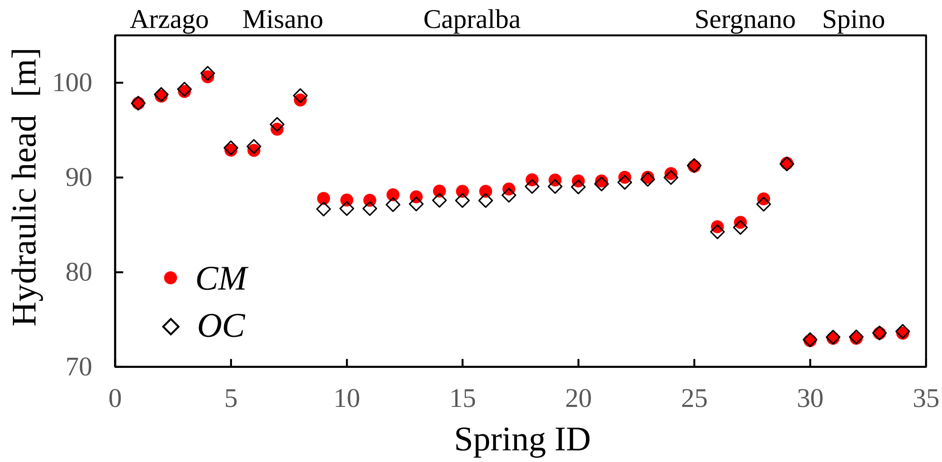

Figure A.2. Simulated hydraulic heads at spring locations for the (a) *Composite Medium* (*CM*; circle) and the (b) *Overlapping Continua* (*OC*; diamond) conceptual modeling approaches.

Appendix B

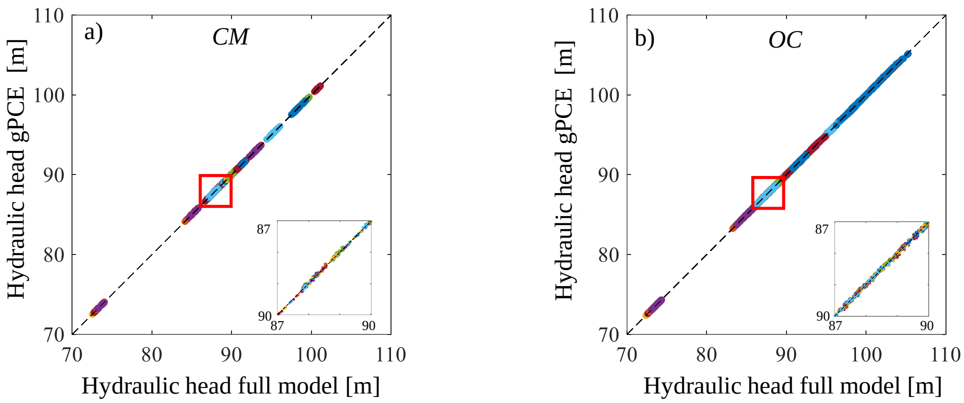

Figure B.1. Head at spring locations evaluated through the generalized Polynomial Chaos Expansion, gPCE, surrogate model versus their counterparts computed with the full model for the N_V = 100 sets of parameter values randomly selected in the parameter space and not employed for the assessment of the gPCE for the (a) *Composite Medium* (*CM*) and (b) *Overlapping Continua* (*OC*) conceptual modeling approaches. Results for each spring location are reported with different colors. The two embedded panels represent a zoom on the region highlighted in red for the two modeling approaches.

Credit author statement

Emanuela Bianchi Janetti: Conceptualization, Formal analysis, Methodology, Writing - original draft, Writing - review & editing. Monica Riva: Conceptualization, Formal analysis, Methodology, Writing - original draft, Writing - review & editing, Supervision, Funding acquisition. Alberto Guadagnini: Conceptualization, Formal analysis, Methodology, Writing - original draft, Writing - review & editing, Supervision, Funding acquisition.

*Declaration of Interest Statement

Declaration of interests

☒ The authors declare that they have no known competing financial interests or personal relationships that could have appeared to influence the work reported in this paper.

☐The authors declare the following financial interests/personal relationships which may be considered as potential competing interests: